REMODEL - Robotic tEchnologies

for the Manipulation of cOmplex

DeformablE Linear objects

Deliverable 6.2 – Force/tactile and pressure/proximity sensors

Version 2021-06-21

Project acronym: REMODEL
Project title: Robotic tEchnologies for the Manipulation of cOmplex DeformablE Linear objects
Grant Agreement No.: 870133
ObjectsTopic: DT-FOF-12-2019
Call Identifier: H2020-NMBP-TR-IND-2018-2020
Type of Action: RIA
Project duration: 48 months
Project start date: 01/11/2019
Work Package: WP6 – Sensory Systems and Mechatronic Tools
Lead Beneficiary: UCLV
Authors: All partners
Dissemination level: Public
Contractual delivery date: 30/06/2021
Actual delivery date: 30/06/2021
Project website address: https://remodel-project.eu

Table of contents

List of figures

1 Scope

This document describes the design and the characterization of the tactile sensors and proximity sensors developed by UCLV for REMODEL project. Concerning the tactile sensor, it is based on optoelectronic technology and a deformable pad with flat surface. Compared to previous developments, the tactile sensor designed for REMODEL has a larger sensing area and a more robust electronic, mechanical, and software design that yields less noise and higher flexibility. A complete characterization for both the single sensing unit and the whole pad is reported to show the potentialities of the sensor in terms of noise, hysteresis, sensitivity, and signal to noise ratio.

Considering the proximity sensors, starting from the tactile sensors, UCLV developed a new pre-touch sensing solution, fully integrated in the pre-existent sensorized fingers, able to recognize the shape of the objects through a specific scanning procedure. This document reports the main design features of the developed proximity sensors, together with its characterization in terms of SNR, repeatability, hysteresis.

A final section is devoted to demonstrate the use of these sensors in simplified scenarios related to REMODEL use cases.

2 Tactile Sensor Technology and Design

The working principle is based on the idea to design an optoelectronic PCB constituted by a discrete number of photo-reflectors (combination of a Light Emitting Diode and a phototransistor), organized as a matrix, suitably assembled with a deformable layer. The objective is to transduce the contact information into deformations measured by the optical sensing points, called “taxels”. The latter, positioned below the deformable layer, provide a “tactile map” corresponding to a spatially distributed information about the contact. Each photo-reflector works in reflection mode: the light emitted by the LED is reflected by the bottom of the deformable layer and comes back to the phototransistor in an amount dependent on the local deformation.

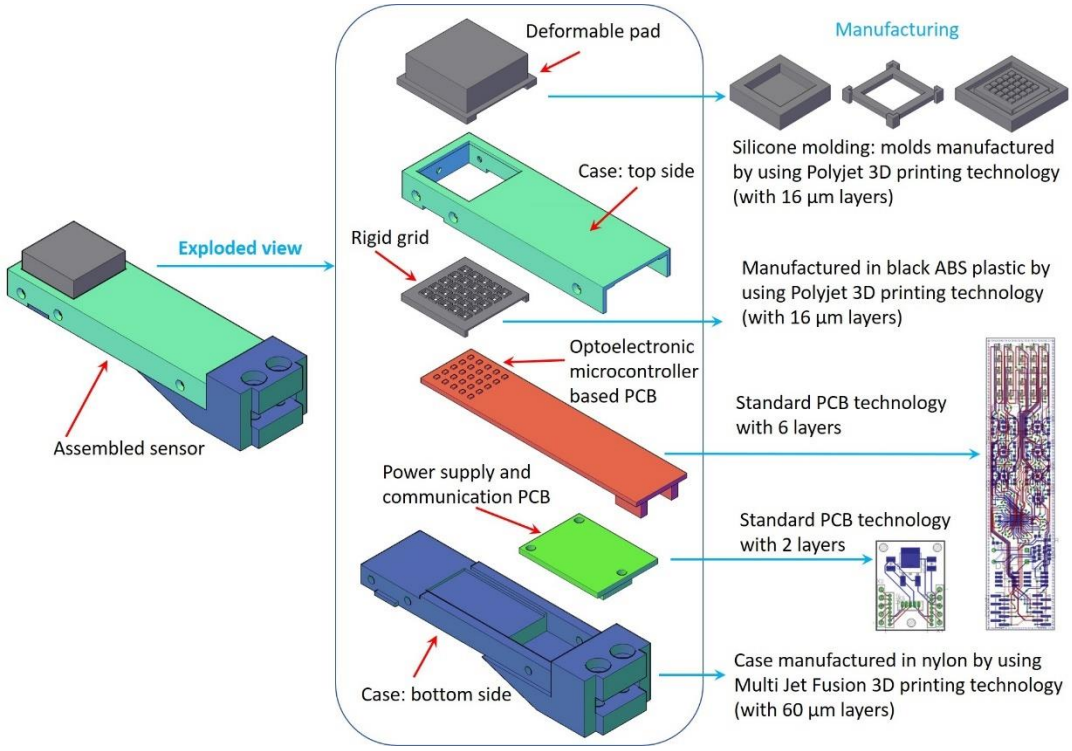

Figure 1: CAD drawing of an assembled sensor (left) with all components (middle) and details about 3D machines used for the production (right).

Figure 1 reports an exploded CAD of all sensor parts, aligned as they have to be assembled. The figure also reports some details about the 3D machines used for the production of mechanical parts.

2.1 Electronic Parts

The electronic core of the sensor is constituted by two PCBs: the main sensing board with the optoelectronic based taxels and a second PCB for the power supplies management and external communication. The main PCB board is constituted by an optoelectronic section with a current driving electronics, a buffering section and a microcontroller, which directly takes care of the analog signals acquisition.The optoelectronic section integrates 25 taxels, organized in a 5x5 matrix, with a spatial resolution equal to 3.55mm. Each taxel is constituted by a photo-reflector (manufactured by New

Japan Radio, with code NJL5908AR) which integrates in the same case an infrared Light Emitting Diode (LED) @925nm and an optical matched phototransistor. The whole taxel matrix, with the selected spatial resolution, corresponds to a sensitive area of about 21x21mm^2. The LEDs are connected in series and they are driven with adjustable current sources (manufactured by Texas Instrument, with code LM334), whose output has been fixed to about 4mA. In order to improve the stability of LED emitted light, a zero temperature coefficient configuration for the current driver has been implemented, by adding a diode and a resistor. By taking into account that this tactile sensor has been designed to be used with commercial electric grippers in robotic applications, during design the availability of a 24V power supply has been hypothesized (typical of robot systems). By considering that the forward voltage of a LED integrated into NJL5908AR is about 1.2V, to drive the 25 taxels, two separate current sources, which use the 24V, have been integrated into the tactile PCB: the first drives 12 LEDs and the second one the remaining 13. Differently, the phototransistors are parallel driven with a 3.3V voltage supply, received from the power supply PCB. Additionally, analogue buffers have been introduced to decouple the phototransistor voltage signals and the Analog-to-Digital converter inputs. The buffering stage has been realized by using low power operational amplifiers (manufactured by Analog Devices, code ADA4691), connected in a standard voltage follower configuration. This stage receives a standard 5V power supply directly from the external connector.The buffer outputs are directly digitalized by using the microcontroller on-board A/D converter, which integrate a sufficient numbers of low noise A/D channels with a 12-bit resolution. The use of this low power microcontroller (manufactured by Microchip, code PIC16F19175) allows a simplification of the interrogation firmware and an enhancement of the signal-to-noise ratio. The power supply of microcontroller is the same 3.3V used for the phototransistors. The serial interface has been selected for the external transmission of measured data, by obtaining a resulting sampling frequency for all 25 taxels equal to 500Hz.

The second PCB has been developed to adapt the sensor interface to different needs, without changing the sensing PCB. The adaptation to several robotic applications with different electric interfaces or available voltage supplies can be implemented by simply modifying this PCB, which is mechanically connected to the sensing PCB though standard connectors. For the presented solution, this PCB presents the microcontroller programming interface and a DC/DC converter used to generate the 3.3V power supply from the external 5V.The scheme of the electronic boards with all connections is shown in the block diagram reported in Figure 2. The manufactured boards, with highlighted components, are reported in Figure 3.

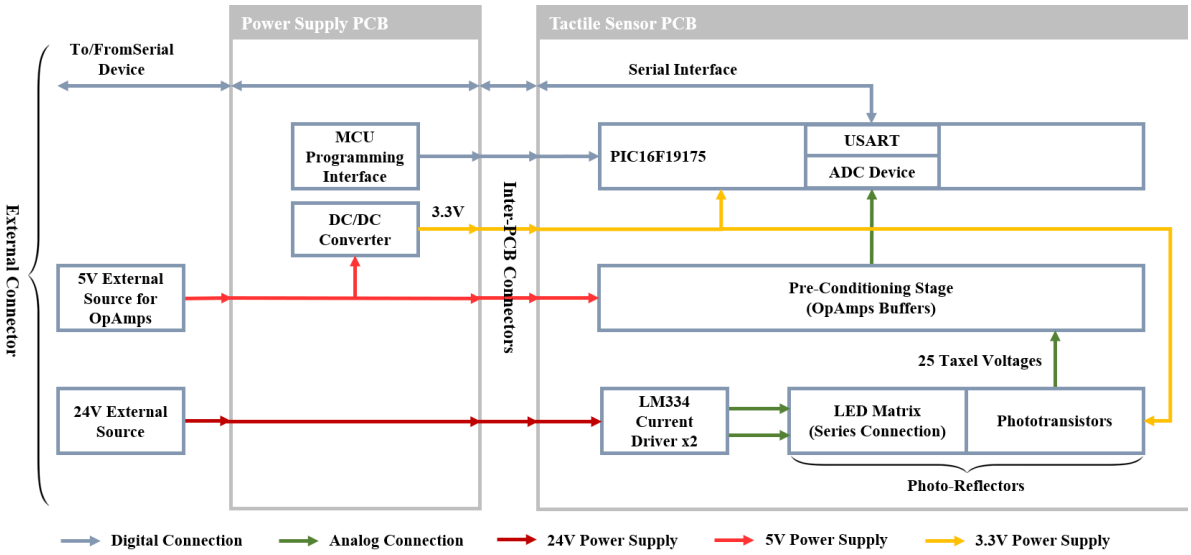

Figure 2: Electronics block diagram.

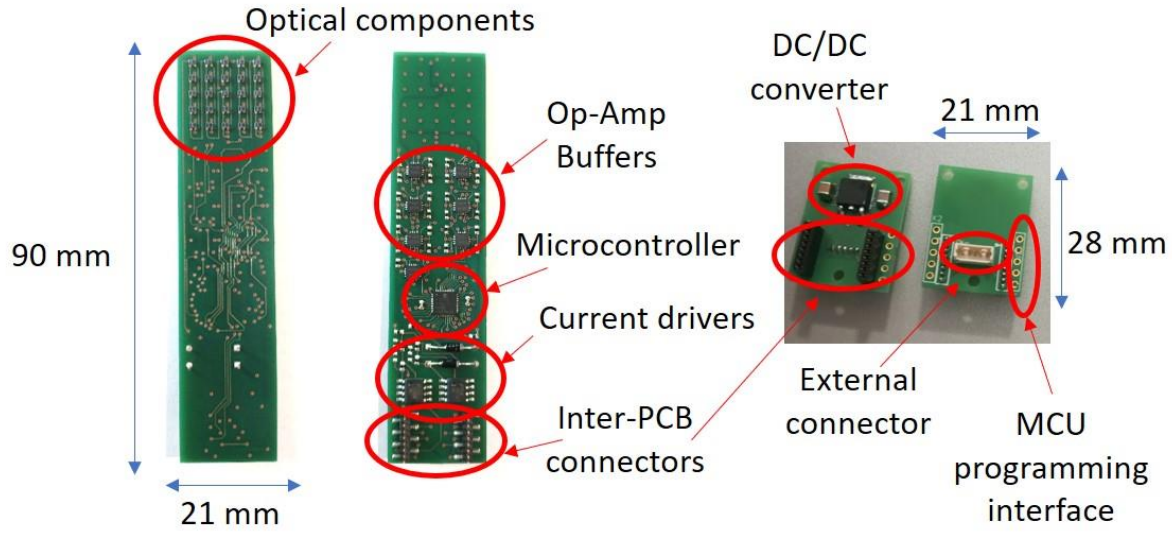

Figure 3: Manufactured PCBs: sensing board (left) and power supply board (right).

2.2 Mechanical Parts

The rigid grid has been designed in order to exploit PCB edges for the mechanical alignment among taxels and reflective surfaces of the deformable pad. For this purpose the grid presents protruding edges on three sides perfectly matched with the tactile PCB, used for the mechanical interlocking among grid and PCB (see Figure 4a). In addition, the grid has the objective to guarantee that the optoelectronic components work in a monotonic range. The grid dimensions, reported in details in Figure 4d, guarantee that the reflective surface cannot reach a distance less than 500µm from the optical components, also if a large deformation is applied to the pad. Finally, the upper side of the grid, designed to be connected with the deformable pad, has grooves to

improve the interlocking robustness among grid and deformable pad. From both sides, the grid is connected with the PCB and the pad by using a cyanoacrylate-based glue. The rigid grid has been manufactured in black ABS plastic by using Polyjet 3D printing technology, with 16μm layers. The color of the grid has been selected to avoid multiple reflections, since black absorbs light.

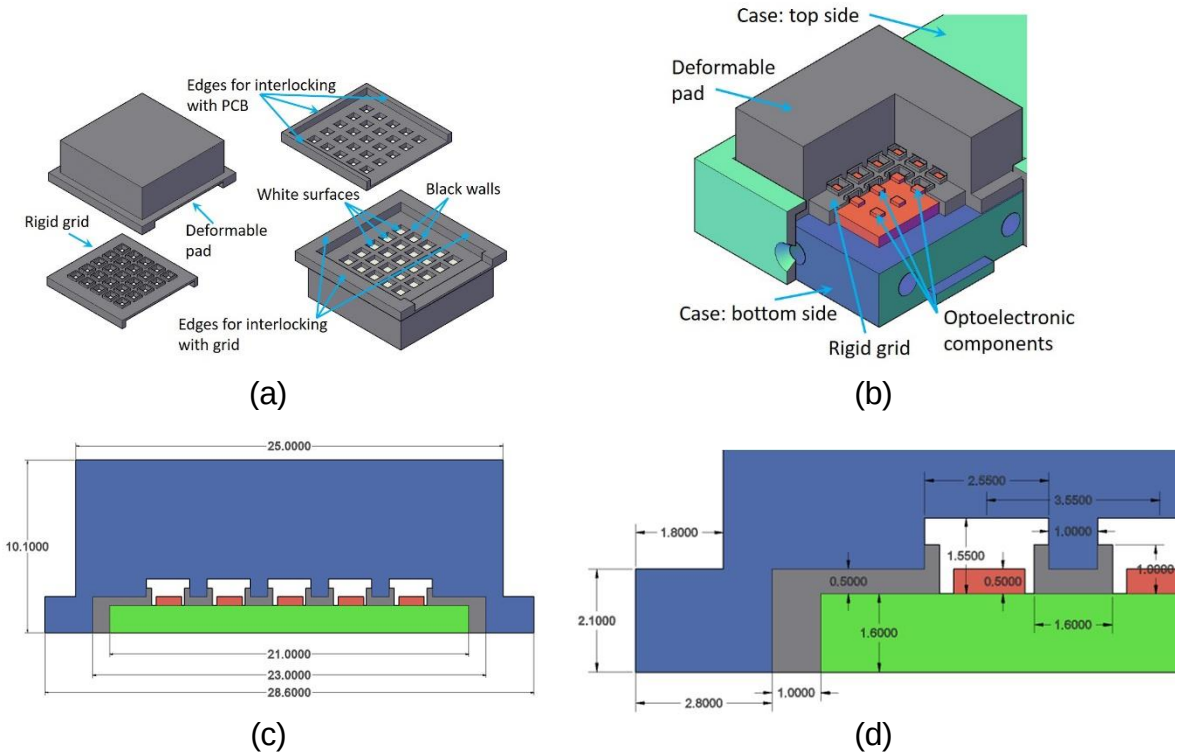

Figure 4: Deformable layer and rigid grid characteristics (a). Mechanical assembly of mechanical and electronic parts (b). Section of the assembled parts with dimensions: full view (c) and zoom view (d).

The deformable pad can be realized with different shapes on the basis of application scenario. For wire manipulation in REMODEL Project a flat surface has been designed. The design also presents a bottom side where suitable cells are realized with white reflective surfaces in front of the optoelectronic components and black walls to optically separate the taxels. Figure 4 reports all dimensions taken from the CAD drawing of the pad, defined for the mechanical matching with the rigid grid. The selected material for the manufacturing is silicone due to its good elastic properties with low hysteresis with respect to other deformable materials. The combination of the two colors (black and white) for the realization is possible only by using the silicone molds technique. Hence, starting from the CAD design of deformable pad, the silicone molds parts shown in Figure 1 have been printed in ABS plastic by using Polyjet 3D printing technology. Then, a silicone dispenser has been used to pour the silicone in the molds in successive layers of different colors. The used silicone is the PRO-LASTIX (manufactured by PROCHIMA, with hardness equal to 20Shore A. The realized grid and deformable pad are shown in Figure 5a and Figure 5b, respectively.

To complete the sensorized finger assembly, a case for housing the tactile sensor has been designed. The case is constituted by two parts: a bottom part thicker and with a precise housing for the electronic boards; a top part used to close the case and to block the deformable layer along its edges. The two parts are mechanically fixed through screws positioned along the side edges of the case, corresponding to the holes shown in Figure 5. The bottom part presents, at the base, two additional holes to fix the assembled sensorized finger to a commercial gripper. The case has been manufactured in nylon by using the Multi Jet Fusion 3D printing technology with 60µm layers. Figure 5c shows a picture of manufactured case parts, while a complete assembled finger is shown in pictures reported in Figure 5d (WSG50 gripper version). Different cases have been designed for the integration of tactile sensors in grippers available in partners' laboratories. In particular, cases for Shunk WSG-50, Panga gripper and OnRobot RG2 have been designed and produced.

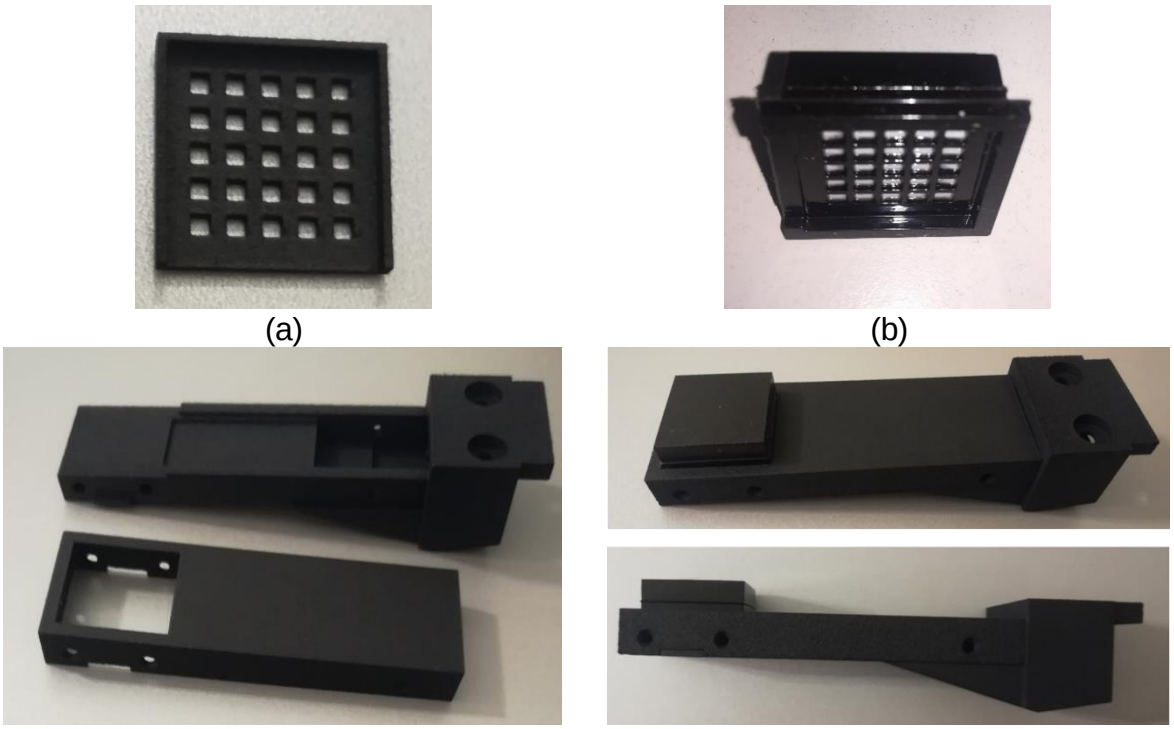

(a) (b)

(c) (d)

Figure 5: Manufactured grid in black ABS (a), deformable layer in silicone (b), case in nylon (c) and complete assembled finger (d).

3 Tactile Sensor Software Design

This section describes the design of the software developed to:

- acquire the taxels information at microcontroller side;
- read and elaborate the data from the tactile sensors at elaboration system side, e.g., PC-based elaboration unit.

3.1 Microcontroller Firmware

At microcontroller (MCU) side, the Firmware has been designed in order to be as much efficient and simple as possible given the high acquisition rate demanded for the tactile sensor interrogation. To enhance the MCU performance all the data processing stages are in charge of the PC-based application. The MCU performs only taxels voltages conversion and sends the digitized data over the serial bus. After an Initialization phase, where the System Devices (System Clock, ADC, Serial interface) are configured, the MCU cyclically executes the operations below:

- it waits a command on the Serial interface;
- it elaborates the command:
    - if the command requests the Sensor ID then the MCU sends its own ID over the Serial bus;
    - if the command requests the Number of the Sensing Elements then the MCU sends the number of taxels over the Serial bus;
    - if the command requests the tactile raw data (i.e., the phototransistor voltages) then the MCU scans each ADC channel and sends the data over the serial bus.

3.2 Elaboration System Software

Concerning the elaboration system application, Robot Operating System (ROS) has been selected as framework for process scheduling and interprocess communication management. The software has been designed in order to be as flexible as possible and independent to the type of sensor and to the number of sensing elements installed on it. Moreover, it is possible to automatically detect the number and the type of the sensors attached to the elaboration system, e.g., PC-based system. This means that the designed SW is able to detect in the initialization phase:

- the number of available serial ports on the PC system;
- the sensor type attached to each serial port (this feature has been used to manage also proximity sensors described below);
- the number of the sensing elements installed on each sensor, e.g., the number of tactile elements (taxels).

Figure 6a reports the flow chart of the designed SW. It can be divided into five main phases:

Serial Port Enumeration: the first step consists in the detection of the available serial devices attached to the Host PC. The SW scans the OS Serial Port handles compatible only with FTDI devices. For example, on Linux OS the serial ports considered during the enumeration phase shall be only the devices recognized with ttyUSB# and ttyACM# under the /dev folder.

Sensor Detection: the second step consists in the detection of the sensors attached to the Host PC via the serial ports previously enumerated. This phase allows to check if a compatible sensor is connected to the serial port and to find the type of the sensor, if it is connected. In Figure 6b the handshake protocol is reported. On the left there are the PC system operations, while on the right, the sensor ones. In order to detect the sensor typology the following steps are executed:

- The Host PC, iterating on all the serial ports enumerated in the first step, sends over serial bus the character “b”;
- If the sensor connected to each serial port is a compatible sensor, it shall send back its Sensor ID;
- The Host PC, once the Sensor ID has been received, collects it in a sensor list. If no Sensor ID is received, the specific serial port is associated to a noncompatible device.

Both tactile and proximity sensors can be managed. In order to properly recognize the Tactile Sensors from the Host PC, the following Sensor ID has been reserved: F### where ### is the number identifier of the sensor, e.g., F001, F013.

Sensor Selection: the third step consists in the selection of one sensor that belongs to the list of compatible sensors previously detected. This operation is demanded to the user that, on the basis of the available sensor list can insert the ID of the device he wants to use.

Sensing Elements Detection: after the user selection, the SW application checks the number of sensing elements installed on the specific sensor. The aim of this task is to:

- automatically detect the presence and the number of available sensing modules on the sensor. For future developments, for example, it should be required to use tactile sensors with a different taxels number depending on the specific task. In the specific design the taxels number is fixed to 25;
- properly set the dimensions of the data buffers used to store the sensor data.

According to the handshake protocol defined in Figure 6b, during this phase the following steps are executed:

- Host PC sends to the sensor the character “c” over the serial bus;
- Sensor answers the Host PC with the number of installed sensing elements;
- If the number of sensing elements equals to zero, then the SW application exits with an error.

Sensor Data Reading: once the sensor has been selected and the number of the sensing elements has been detected, the SW application proceeds with the sensor data reading. According to the handshake protocol of Figure 6b, in order to read the sensor data the following steps are executed:

- Host PC sends to the Sensor the character “a”;
- Sensor answers sending back the RAW data.

For tactile sensors the RAW data correspond to the phototransistors voltages, which are codified with an unsigned integer of 16 bits and then converted in a decimal number through a specific transduction constant.

By exploiting the described SW architecture, it is possible to acquire the whole 5x5 sensor matrix, i.e., the 25 taxel voltages, with an average sampling frequency of 500Hz and a standard deviation of 13.12Hz. The latter has been computed by using the ROS Topics tools and by considering a time window of one minute. It has to be noticed that the presented performance is reached by using a standard no Real-Time Linux-based OS and a middle-level microcontroller.

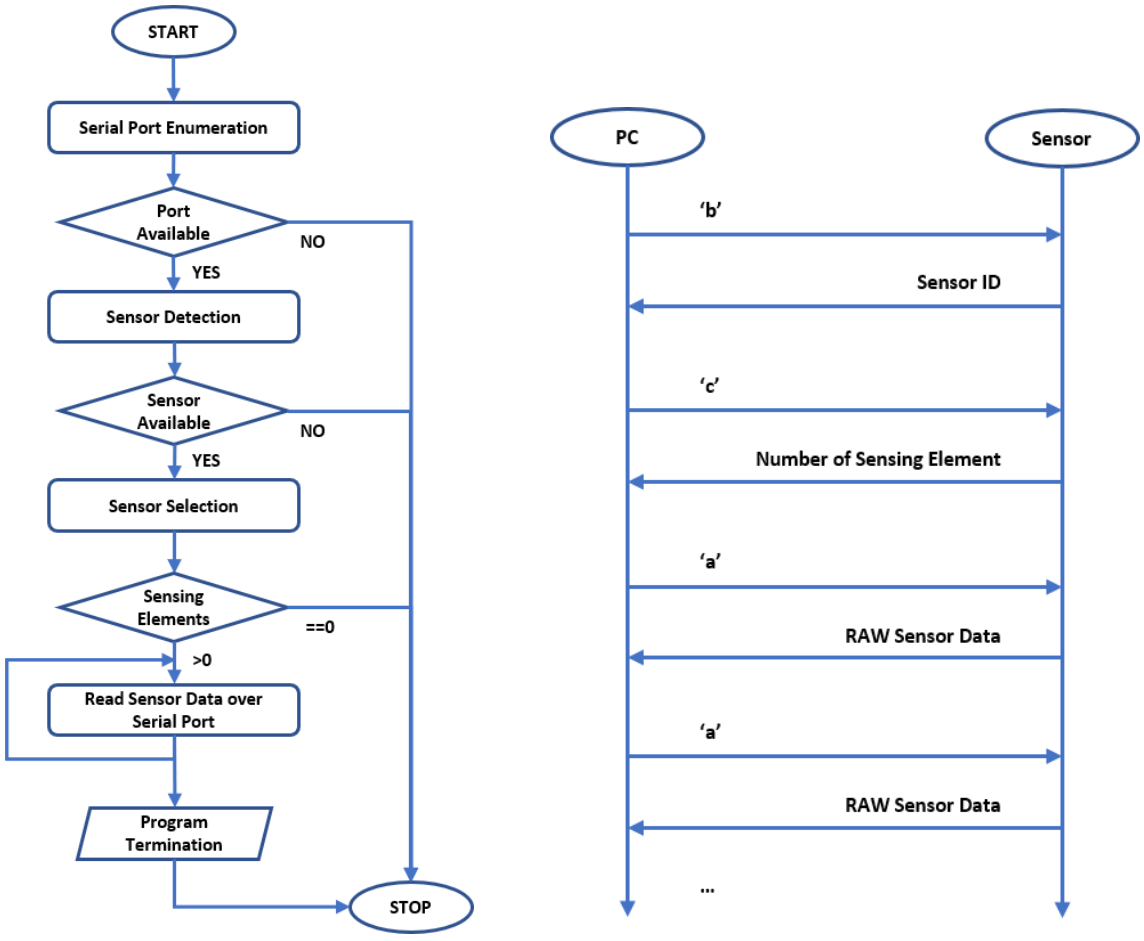

(a) (b)

Figure 6: Elaboration system software design: software flow chart (a) and protocol sequence diagram (b).

4 Tactile Sensor Characterization

By considering the sensor structure, it is useful to characterize both a single taxel and the whole pad in order to evaluate sensor performance in different working conditions. For example, the manipulation of wires involves the use of only a limited number of taxels along a line, while the manipulation of boxes involves the use of the whole pad.

4.1 Single Taxel Characterization

In order to assess some properties for the single taxel (e.g., hysteresis, Signal-to-Noise Ratio, repeatability, response time), several experiments have been carried out on different taxels, since the mechanical properties are slightly dependent on the taxel position in the pad, due to silicone amount surrounding it. A 6-axis force/torque sensor has been used as a reference sensor to acquire the normal force applied to the tactile sensor together with the voltage variation signals coming from the tactile sensor itself.

The setup for the experiments is reported in Figure 7a where it is possible to distinguish four elements:

- the force/torque sensor;
- the tactile sensor;
- a mask;
- an external object.

The force/torque sensor used as reference sensor in the experiments is a Robotous RFT40-SA01. The mask is a 3D-printed piece used to find easily the points where to press on the silicon pad and it has three holes in correspondence of the taxels considered in the experiments, which are the taxels 5, 13 and 17 (numbering of taxels is in Figure 7b). The taxels have been selected on the basis of their position: the central one, one on an edge and one in an intermediate position. The external object is a thin tool used to press on a single taxel of the tactile sensor and it is connected to an UR5e robot manipulator in order to achieve high repeatability during the experiments for the different taxels.

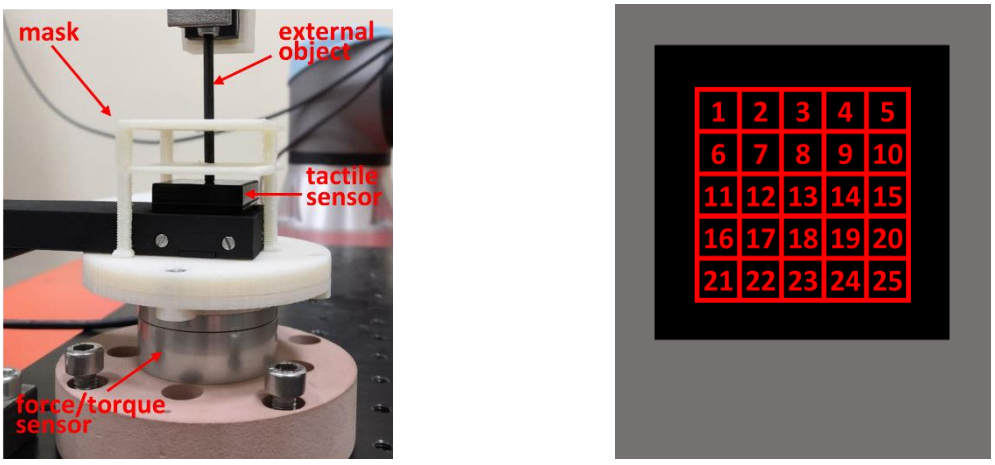

(a) (b)

Figure 7: Experimental setup for single taxel (a) and taxel numbering used in the experiment description (b).

Hysteresis. To evaluate the hysteresis of the taxels, the silicon pad has been preset by using a thin object with a speed of 1.5mm/min and then released with the same speed. The robot pose and velocity have been controlled through the robot interface. Voltage variations and force signals acquired during this experiment for the taxel 17 are reported in Figure 8 with respect to the time in order to show the very low speed used to guarantee to highlight only static hysteresis (data for taxels 5 and 13 are similar). The hysteresis graph has been obtained by plotting the force values on the x-axis and the voltage values on the y-axis. The hysteresis error has been computed by finding, for each taxel, the maximum difference between the voltage variation values on the two hysteresis branches, corresponding to the same force value, by using the following equation:

$$e_{hyst} = \frac{|\Delta v_{incr} - \Delta v_{decr}|}{v_{max}} \times 100 \quad (1)$$

where Δv_{incr} and Δv_{decr} are the voltage variation values on the increasing and decreasing force sides respectively and v_{max} is the maximum voltage value reached during the experiment. Figure 9 shows the hysteresis graphs and errors for taxels 5, 13 and 17 respectively. It is possible to see how the three taxels have similar hysteresis errors (the maximum voltage value is 0.4V and is the same in all the three experiments). In particular, the hysteresis error is 4.34% for the taxel 5, 4.53% for the taxel 13 and 4.83% for the taxel 17. The low hysteresis values are in accordance with the mechanical properties of the silicone used to realize the deformable pad.

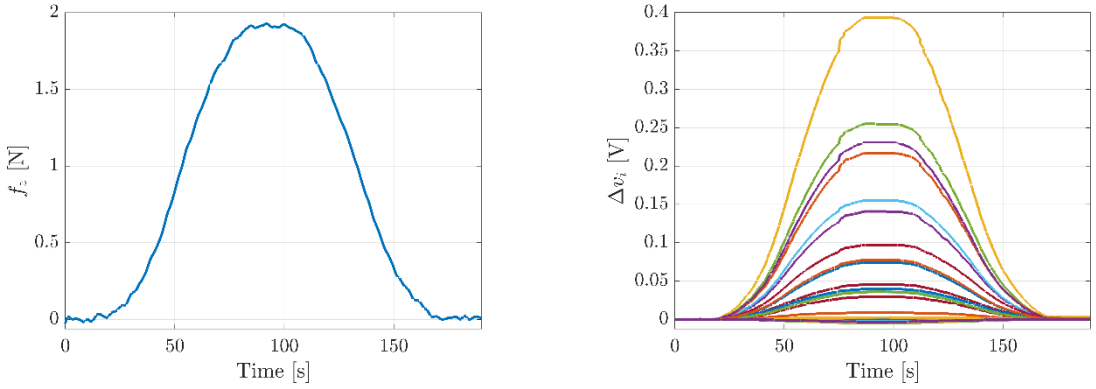

(a) (b)

Figure 8: Hysteresis experiment for taxel 17: applied force (a) and voltage variations (b).

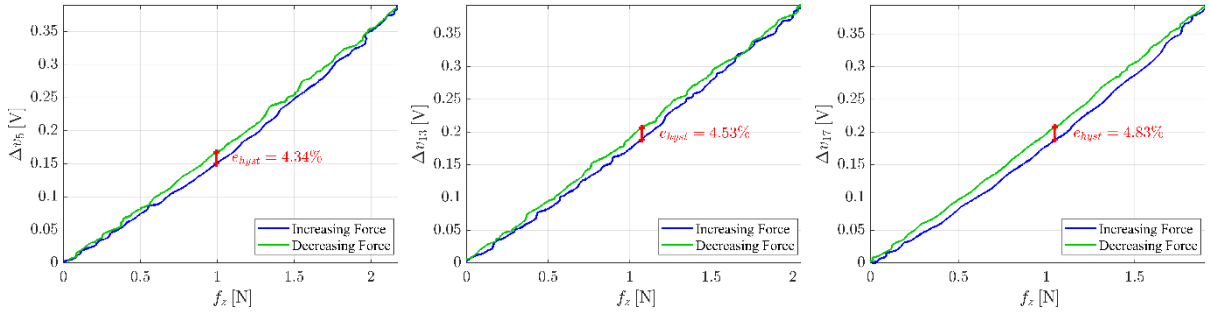

(a) (b) (c)

Figure 9: Hysteresis graphs for taxel 5 (a), taxel 13 (b) and taxel 17 (c).

Repeatability. The repeatability error has been evaluated by repeating the same experiment carried out for the hysteresis two times consecutively, as shown by force and voltages data reported in Figure 10. The two rising edges have been compared, by reporting on the graphs the force values on the x-axis and the voltage values on the y-axis. The repeatability error is computed considering the two most different voltage values corresponding to the same force value. The formula used, for each taxel, in this case is:

$$e_{repeat} = \frac{|\Delta v_a - \Delta v_b|}{v_{max}} \times 100 \quad (2)$$

where Δv_a and Δv_b are the voltage variation values on the two rising edges and v_{max} is the maximum voltage value reached during the experiment. Figure 11 shows the repeatability errors for taxels 5, 13 and 17 respectively. The error in the three cases is almost the same and is about 3%, by demonstrating the high repeatability for the proposed design.

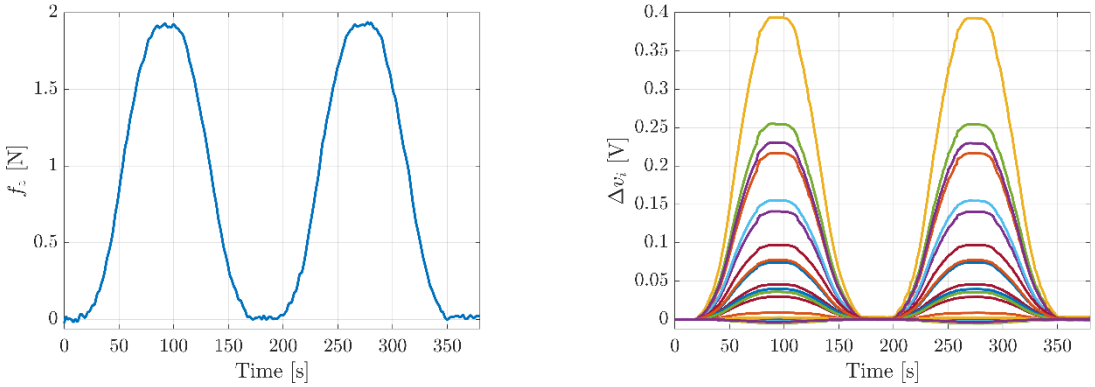

(a) (b)

Figure 10: Repeatability experiment for taxel 17: applied force (a) and voltage variations (b).

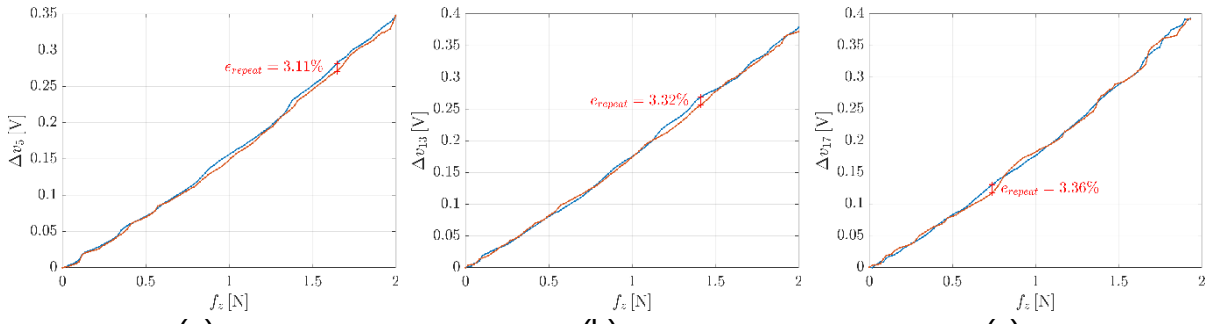

(a) (b) (c)

Figure 11: Repeatability error graphs for taxel 5 (a), taxel 13 (b) and taxel 17 (c).

Response Time. The experiment for the evaluation of the response time consists in a step variation in the position of the external object, hence in a step variation of the voltage values. In this case, the voltage signal has been compared to the position along z-axis of the robot end-effector (the external object) and not to the force signal because the latter is affected by the delay due to the elasticity of the silicon layer of the tactile sensor. The response time has been evaluated measuring the time distance between the normalized voltage and the normalized position picked at half step. Figure 12 shows the results of the experiment for the taxel 5, 13 and 17, respectively. The response time is 0.0092s for the taxel 5, 0.0087s for the taxel 13 and 0.0098s for the taxel 17, so it is less than 0.01s in all the three considered cases.

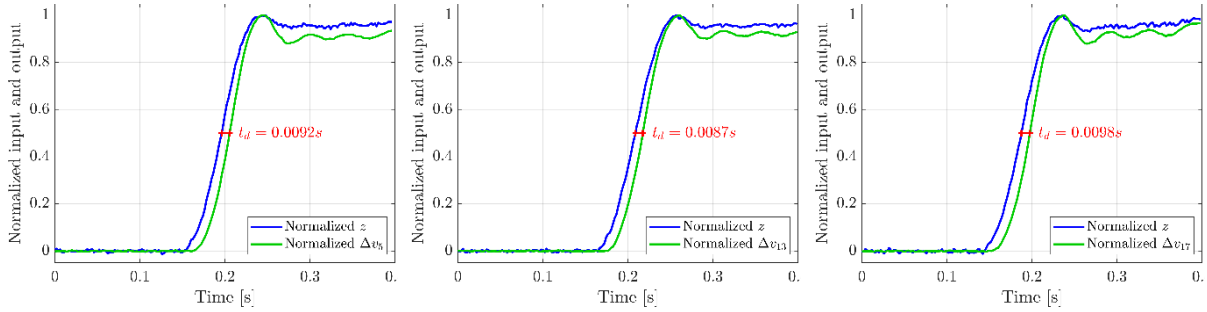

(a) (b) (c)

Figure 12: Response time graphs for taxel 5 (a), taxel 13 (b) and taxel 17 (c).

Signal-to-Noise ratio. The power spectrum of the voltage signals for the three taxels have been computed to evaluate the SNR. The results for the three taxels are reported in Figure 13 where it is possible to see that, since the bandwidth of the signals of interest is limited to few hertz, the noise level is about 5-6 order of magnitude below the signal level. The optimal result in terms of SNR is mainly due to the current driven solution implemented for the LED.

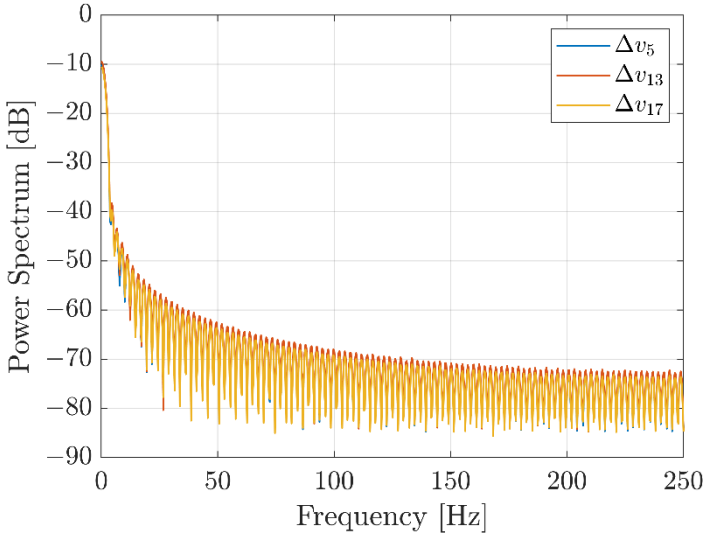

Figure 13: Power spectrum of taxels 5, 13 and 17.

4.2 Whole Pad Characterization

The previous section investigated the properties of the single taxel, while this section is devoted to characterizing the properties of the whole sensor, by considering working conditions in which all taxels are involved at the same time. In particular, experiments, where the whole pad has been deformed along the normal direction, have been implemented. In this case the normal force is related to the sum of all taxel measurements. The evaluation of sensor performance has been carried out by comparing the applied normal force to the mean of voltage variations, measured by taxels, according to the following equation:

$$\frac{1}{25}\sum_{i=1}^{25}\Delta v_i \tag{3}$$

The experimental setup is represented in Figure 14 and it is conceptually similar to the previous one. This time the reference 6-axis force/torque sensor is an ATI NANO43. The whole tactile sensor is stimulated by a flat tool attached to a MECA500 robot, in this way the applied force is distributed over the whole pad. The robot is commanded to apply specific normal force profiles to the sensor pad. The use of a different setup proved useful, because the stimulation of all taxels at the same time and by applying a normal force as uniform as possible was not easy to reach with the previous setup. To simplify the goal achievement, a higher precision for the alignment among the contact plane and the flat surface of the deformable pad was needed. For this reason, the Meca500 with a repeatability equal to 0.005mm has been used together with the ATI force/torque sensor.

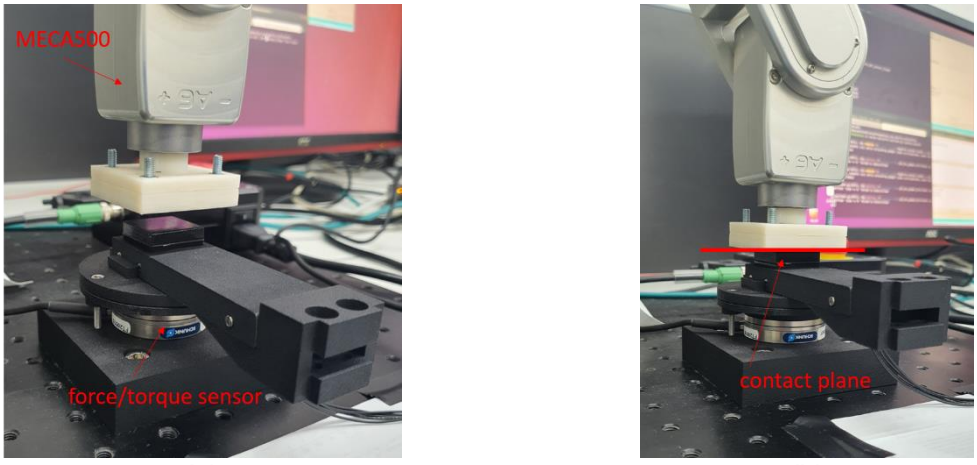

(a) (b)

Figure 14: Experimental setup for the whole pad characterization: components (a) and contact example (b).

Hysteresis. The pad has been pressed with a sequence of force profiles at various speeds. Figure 15 shows the normal force applied to the pad and the corresponding voltage variations. In particular, four different force profiles have been applied at 0.2, 0.4, 0.8 and 2.0N/s, respectively. The different speed has been used also to evaluate if the sensor hysteresis is purely static. During the experiments, for every value of the force speed, the maximum force value of 15N has been repeatedly reached. Obviously, the applied force

necessary to obtain deformations (hence voltage variations) similar to a single taxel is higher, due to the contact area extension.

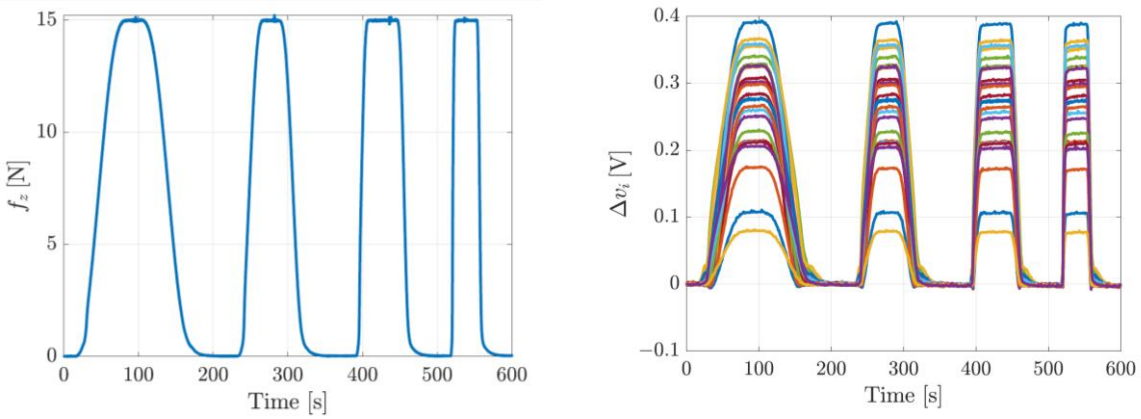

(a) (b)

Figure 15: Hysteresis experiment for the whole pad characterization: force profile (a) used to stimulate the pad and corresponding voltage variations (b).

Figure 16 shows the hysteresis graph for taxel 5 (taken as single taxel example) and for the voltage mean computed as in Equation (3). The hysteresis is evaluated by using the same algorithm in Equation (1). The experiment shows how hysteresis is practically the same of the single taxel characterization, particularly if in this case the maximum reached force is much higher. Both the comparisons for a single taxel (the number 5) and for the mean of all voltages, at low speed (between 0.2 and 0.4N/s), show a hysteresis limited to 5-6%. The slight increase with variation rate of applied force is related to a simple phase delay introduced by the linear filtering effect due to an equivalent spring-like system representing the soft sensor pad.

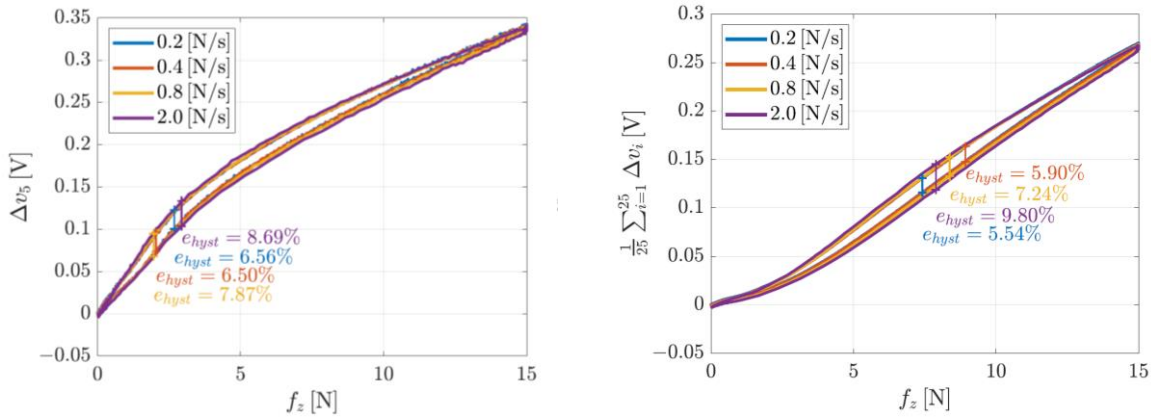

(a) (b)

Figure 16: Hysteresis graph for the whole pad characterization: a single voltage (a) and mean of voltages (b).

Repeatability. The repeatability error for the whole sensor pad has been evaluated in a similar fashion to the previous case and by using the same Equation (2). Figure 17 shows the result both for taxel 5 and the mean of all voltages. Because the applied force is distributed over the whole contact area, the reached voltage values are similar to the

previous repeatability experiment, even if the reached normal force is higher. Moreover, by stimulating the sensor with such a distributed contact, a better repeatability error (about 1.32%) is reached and it is even better if all the voltages together are considered (0.81%).

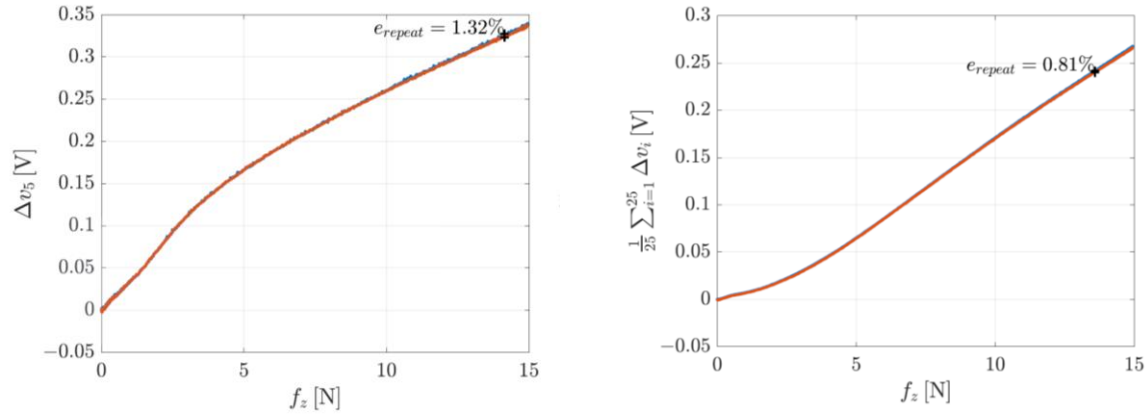

(a) (b)

Figure 17: Repeatability graph for the whole pad characterization: a single voltage (a) and mean of voltages (b).

Sensitivity. This section describes an experiment devoted to show the sensitivity of the tactile sensor with respect to the increments of the normal force. During the experiment, starting from an applied force of 0.35N, additional weights corresponding to a normal force of about 0.1N have been iteratively added. Hence, the comparison of the normal force and the mean of the voltages of all taxels has been considered and reported in Figure 18. The sensitivity can be evaluated by means of linear interpolation. The obtained sensitivity is about 0.018V/N considering the mean of all measured voltages.

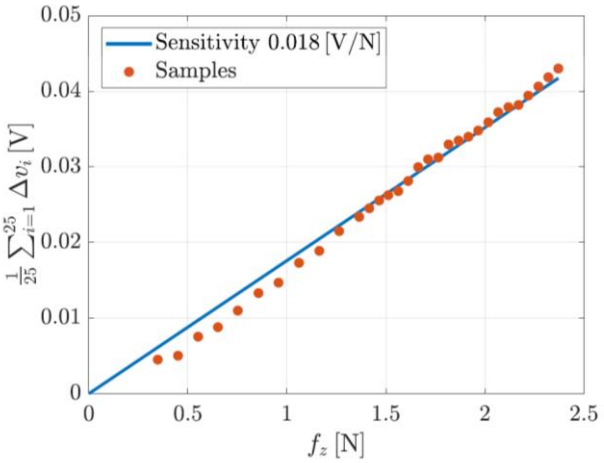

Figure 18: Sensitivity graph for the whole pad characterization.

5 Proximity Sensor Technology and Design

This section describes the mechanical, software and hardware design of the proposed prototype. Starting from the tactile sensor described above, the pre-touch (proximity) sensor prototype has been designed in order to be compatible with the existing tactile sensor solution from both mechanics and hardware/software point of views. In particular, the compatibility of the new sensors with the mentioned tactile one represented the principal design constraint, e.g., the new board has been designed in such a way it can be installed on the rear side of the tactile sensor and respecting the electrical and software interface of the latter. The choice of a reliable, accurate, but also small-sized proximity sensor is mandatory in order to not significantly alter the shape and dimensions of the tactile sensor chassis. Given the previously listed requirements, the VL6180X Time-of-Flight sensor provided by STMicroelectronics has been chosen. The ideas behind the integration of proximity sensors on the tactile finger are twice: a) to detect unknown objects in the surroundings of the latter when a robotic arm, where the tactile sensor is installed on, is performing a pick and place task, b) to estimate the position and the shape of close objects, i.e., thin wires, that the robotic gripper has to grasp and manipulate. Proximity sensors have to be placed along different axis in order to detect objects in all the directions, see Figure 19. From that, the need of designing small and multiple proximity sensor modules which can be installed, with a Plug&Play procedure, on the existent tactile sensor using small and non-invasive connectors and PCBs.

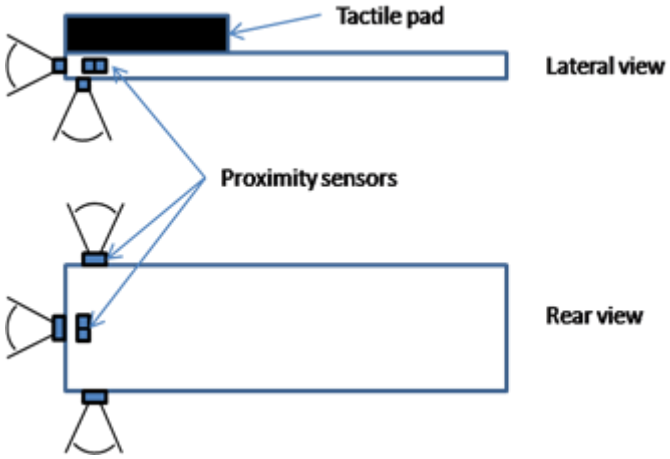

Figure 19: Sketch of the Tactile Sensor with Proximity Sensors.

5.1 Mechanical Design

The mechanical design started from the CAD drawings of the tactile sensor case. In order to cover four directions around the tactile sensor with the proximity module Field of View (FoV) and given the limited space available on the pre-existent cases of the tactile sensor, i.e., 25x45mm, specific connection solutions has been detected. The chosen connectors allow to install new and small PCBs forming 90 degrees w.r.t. the tactile sensor case by guaranteeing a low height profile of the pre-existent case, i.e., new electronics can be embedded in 10mm height-sized box. In fact, with the detected components, it is possible to design proximity sensor modules with very small PCBs, i.e., 12x8mm. See Figure 20 for the CAD drawings.

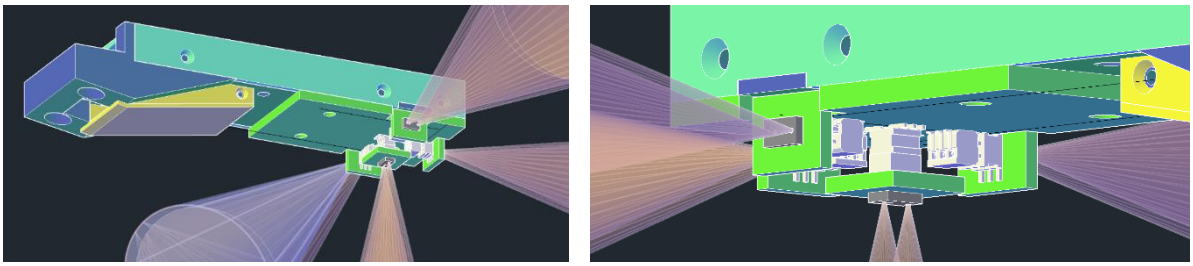

(a) (b)

Figure 20: CAD Drawings of the proximity sensor modules

For more details, below the part number of the connectors are listed:

- Samtec CLP-103-02-F-DH: female horizontal low profile connector,
- Samtec FTSH-103-04-F-DV: male vertical connector (compatible with CLP-103-02-F-DH),
- Samtec CLP-103-02-F-D: female vertical low profile connector,
- Samtec FTSH-103-03-F-DV: male vertical connector (compatible with CLP-103-02-F-D).

5.2 Hardware Design

This section describes the design of the system from a Hardware point of view. The electronics has been developed in order to separate the pre-touch system into two parts:

- an interface board, to allocate rear the tactile sensor chassis,
- a self consistent sensor module, that hosts the VL6180X.

According to the specific need to have or not locally a dedicated processing unit, the interface board has been designed into two version. The first one (v1) represents only an adapter, a kind of bridge, between the proximity sensor modules and the interrogation board of the tactile sensor. The board, 24x23mm of dimensions, is able to host up to four proximity sensor modules through horizontal connectors and can be connected to the tactile board via a 8-ways connector, i.e., JST SM08B-SRSS-TB. Figure 21a reports the Eagle view of the designed 2-layers PCB.

The second version (v2) of the interface board provides a complete, compact (24x34mm) interrogation system for the proximity sensor modules. As the first version, it can host up to four proximity modules, but it provides also an elaboration unit for sensor data acquisition. The MCU is a PIC microcontroller, i.e., PIC16F19176. The microcontroller can be externally interrogated through a Serial Bus via the 5-ways interface connector, while it scans the proximity sensor modules via I2C interface. Differently from the v1, in the v2 the middle proximity module is directly soldered on the PCB and it is no more connected through the connector. Moreover, the board provides the programming connector that can be used to flash the PIC firmware via PicKit 3 programmer. Figure 21b reports the Eagle view of the designed 2-layers PCB.

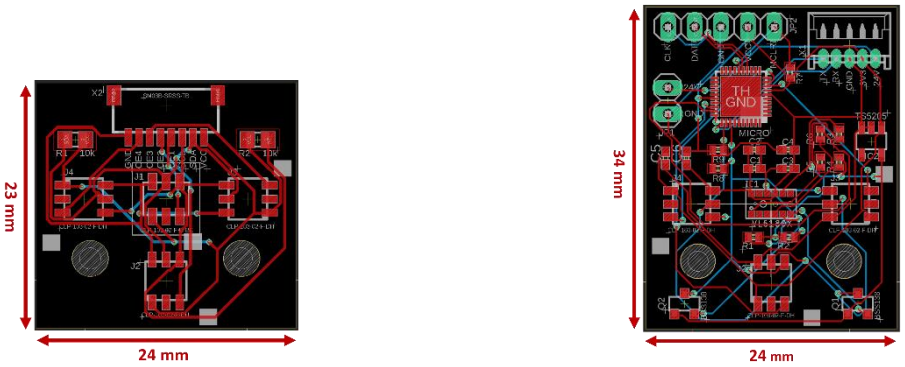

(a) (b)

Figure 21: Interface board v1 (a) and v2 (b): Eagle view of the PCBs.

Concerning the proximity sensor module, it has been designed in order to obtain a self consistent module. The module PCB hosts all the components needed to properly communicate with the VL6180X device and to supply it: a LDO Regulator, i.e., TPS76928, is used to provide the 2.8V to the sensor, while two BSS138 are used as level shifters to adapt the logic levels for the I2C bus. The module dimensions are only 12x8mm and it can be accessed via a 6-ways Samtec connector, namely, the Samtec FTSH-103-04-F-DV. Figure 22a shows the Eagle view of the PCB of the proximity sensor module, while Figure 22b and Figure 22c show the top and bottom perspective of the complete proximity sensor module. Figure 23 reports a view of the complete system composed by the Interface Board (v1) and two proximity sensor modules integrated on the same finger that hosts the tactile sensor.

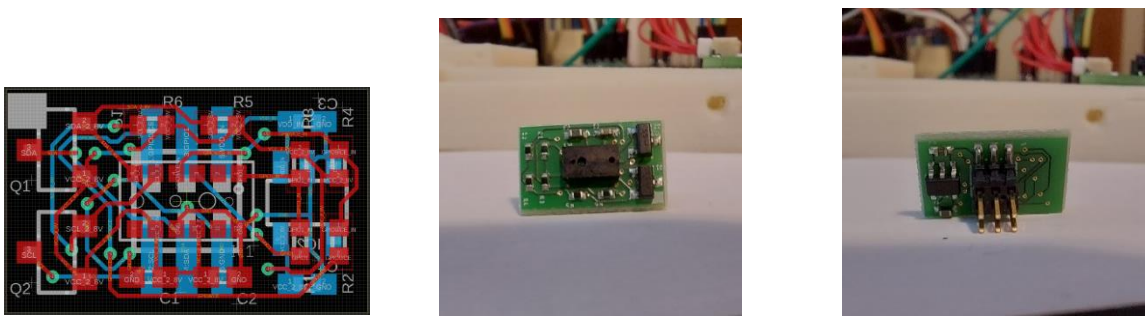

(a) (b) (c)

Figure 22: Proximity sensor module: Eagle view of the PCB (a), top (b) and bottom (c) view of a realized module.

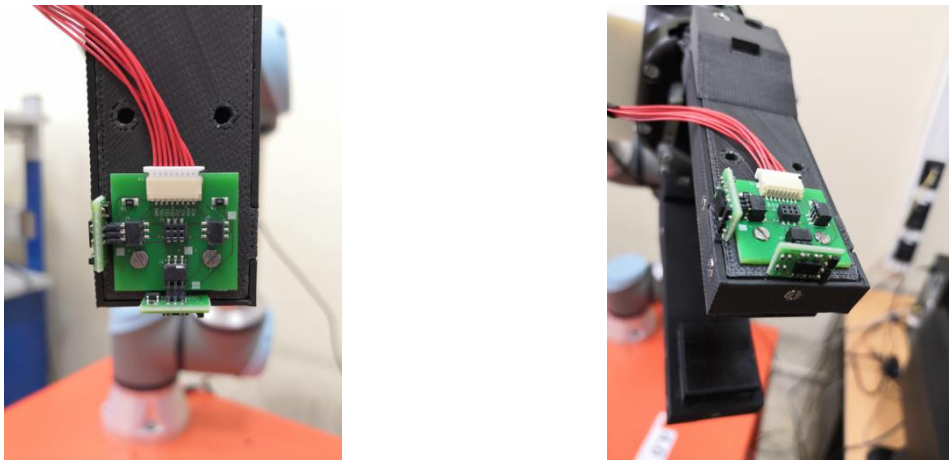

(a) (b)

Figure 23: Interface board v1 and two proximity sensor modules installed on the tactile finger.

5.3 Software Design – MCU side

The VL6180X is a Time of Flight proximity sensor that communicates with a microcontroller system through a serial I2C bus (it represents a slave device). The communication protocol is not a standard one, so a custom I2C low level driver for read and write operation needs to be developed. As described above, the chosen elaboration unit is a Microchip PIC16F19175/176 microcontroller, so the Microchip MPLab IDE and XC8 compiler has been chosen as firmware development toolchain. According to its datasheet, the VL6180X has different registers that can be used to:

- configure the range measurement functionality,
- configure the ambient light sensor measurement functionality,
- configure the convergence time,
- configure the measurement period,
- read the sensor measurements.

In order to access to the mentioned registers the I2C protocol reported in Figure 24 has to be implemented, where 'S' is the start bit, 'As' is the acknowledge of the slave device, 'Am' is the acknowledge of the master device, 'P' is the stop bit. An high level API library has been developed in order to allow easily the user to configure the device and read the range measurements. The APIs are listed below:

- uint8_t VL6180X_IdentifyDevices(void): identifies the number of VL6180X devices on the I2C bus,
- void VL61800X_SetChipEnable(uint8_t DeviceNumber): enables the device through the dedicated GPIO microcontroller pin,
- bool VL6180X_WriteRegister(uint8_t address, uint16_t reg, uint8_t data): writes a device register,
- uint8_t VL6180X_ReadRegister(uint8_t address, uint16_t reg, bool error): reads a device register,

- void VL6180X_SetupRegisters(uint8_t DeviceNumber): setups all the configuration registers of the device,
- void VL6180X_MeasureRange(uint8_t NumDeviceToRead, uint8_t measure, uint8_t status): read the range measurements of the devices on the I2C bus.

A typical application should call in sequence the following routines in order to properly accomplish a range measurements:

1. VL6180X_IdentifyDevices(),
2. VL6180X_SetupRegisters() for each detected device,
3. VL6180X_MeasureRange() for one range measurements.

The specific SW implementation allows to plug and unplug the proximity sensor modules without any SW modification or re-compilation. Once the number of proximity modules changes, it is enough to restart the MCU in order to automatically re-configure it. The developed SW library is free available to the read at the repository https://github.com/Vanvitelli-Robotics/REMODEL_WP6_MDPI_SENSORS_2021.

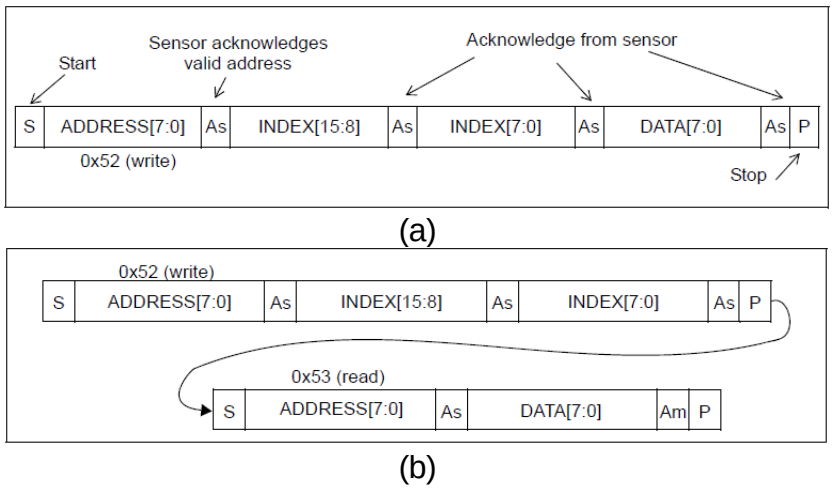

Figure 24: Write (a) and read (b) register operations.

5.4 Software Design – PC side

Concerning the design of the software developed to read and elaborate the data from the proximity sensors, it is the same described for the tactile sensors. As detailed above, the software has been designed in order to be as much flexible as possible and independent to the type of sensor (both proximity and tactile sensors are compatible) and to the number of sensing elements installed on it. Also in this case, despite the particular protocol used for data exchange, it is possible to automatically detect the number and the type of the sensors attached to the elaboration system, e.g., PC-based system. It means that the designed SW is able to detect in the initialization phase:

- the number of available serial ports on the PC system,
- the sensor type attached to each serial port: tactile or proximity sensor,

- the number of the sensing elements installed on each sensor, i.e., number of taxels for tactile sensors or VL6180X modules for proximity sensors.

Once the initialization phase has been completed, the proximity sensor RAW data are made available on a ROS topic, namely, '/sensor_data' topic. The RAW data correspond to the distance (not filtered signal), in millimeters, from the observed object. The distance is codified with an unsigned integer of 8 bits (uint8_t) and the maximum reading frequency reached with the presented system is 50Hz for each proximity module. With the configuration used in this specific application the proximity sensor is able to measure the distance from an object with millimetric accuracy in a range of 0.5mm to 100mm.

6 Proximity Sensor Characterization

This section reports the sensor characterization in terms of repeatability, hysteresis, SNR, sampling frequency. In order to provide a complete overview of the designed system, the developed proximity sensor and the interrogation board based on the PIC MCU have been compared with the on-hand ST solution. The characterization and the comparison analysis show the effectiveness of the proposed solution.

From a Software point of view the ST solution provides:

- a Windows-based application (VL6180X_Explorer) with a graphic interface that allows to visualize online the sensor data, e.g., range in mm, ALS data, frequency, and to log the acquired data in CVS format;
- a Firmware compatible with the Windows application and the STM32F401 Nucleo Board.

Figure 25 reports how the sensor data are acquired with both systems. In the upper diagram a schematization of the operating phases for the ST solution is reported, while in the lower one there are the operating phases for the designed solution. It is clear how the ST solution does not allow to read the raw sensor data. In fact at PC Application level only filtered data are available. In particular, the sensor data are processed by two filtering steps:

- a low pass filter (LPF) is implemented at firmware level. The output of the LPF is provided to the PC Application;
- a filtering process based on the SNR is implemented at application level. When the SNR of a single sample is too low then the sample is discarded.

The second filtering step is necessary in order to obtain a clean ranging signal. Given the low level driver configuration of VL6180X device for the ST solution, the acquired data not always are correct due to high convergence time and low SNR. Figure 26 shows in the upper image:

- in blue the data not processed with the second filtering stage,
- in red the data processed with both filtering stages.

While in the lower image, the SNR acquired from the PC ST Application is reported. The red curve is obtained selecting the samples of the blue curve by thresholding the SNR. In particular, if a specific sample in output to the LPF has a SNR lower than 255 then the sample is discarded.

Concerning the custom solution, the SW does not implement any filtering stage, so all the analysis are made on the raw sensor signal.

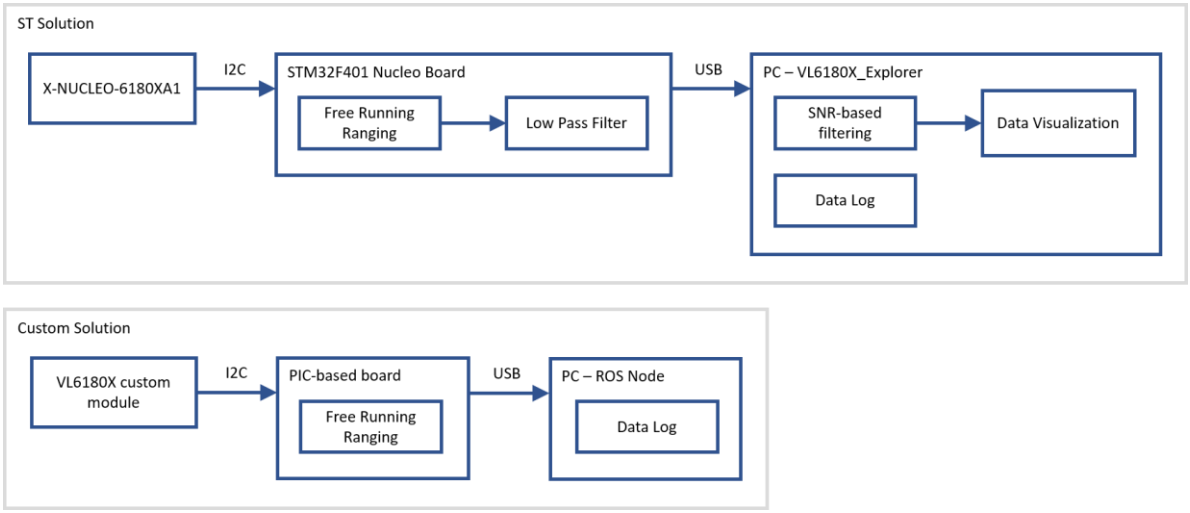

Figure 25: SW operating diagrams.

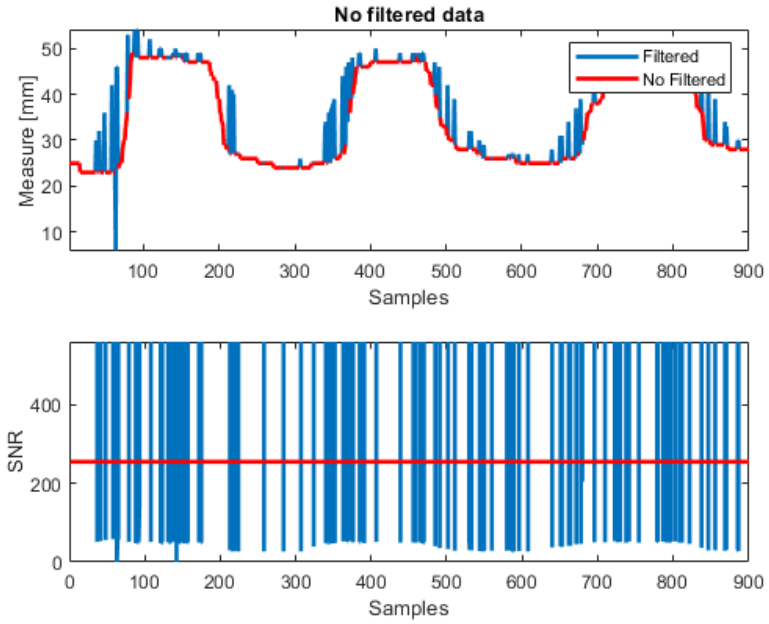

Figure 26: SNR Filtering stage for ST Solution.

Figure 27 reports the characterization setup for the two solutions. A box is used as object and a standard meter to measure the object distance from the sensor. Same setup is used for both systems characterization.

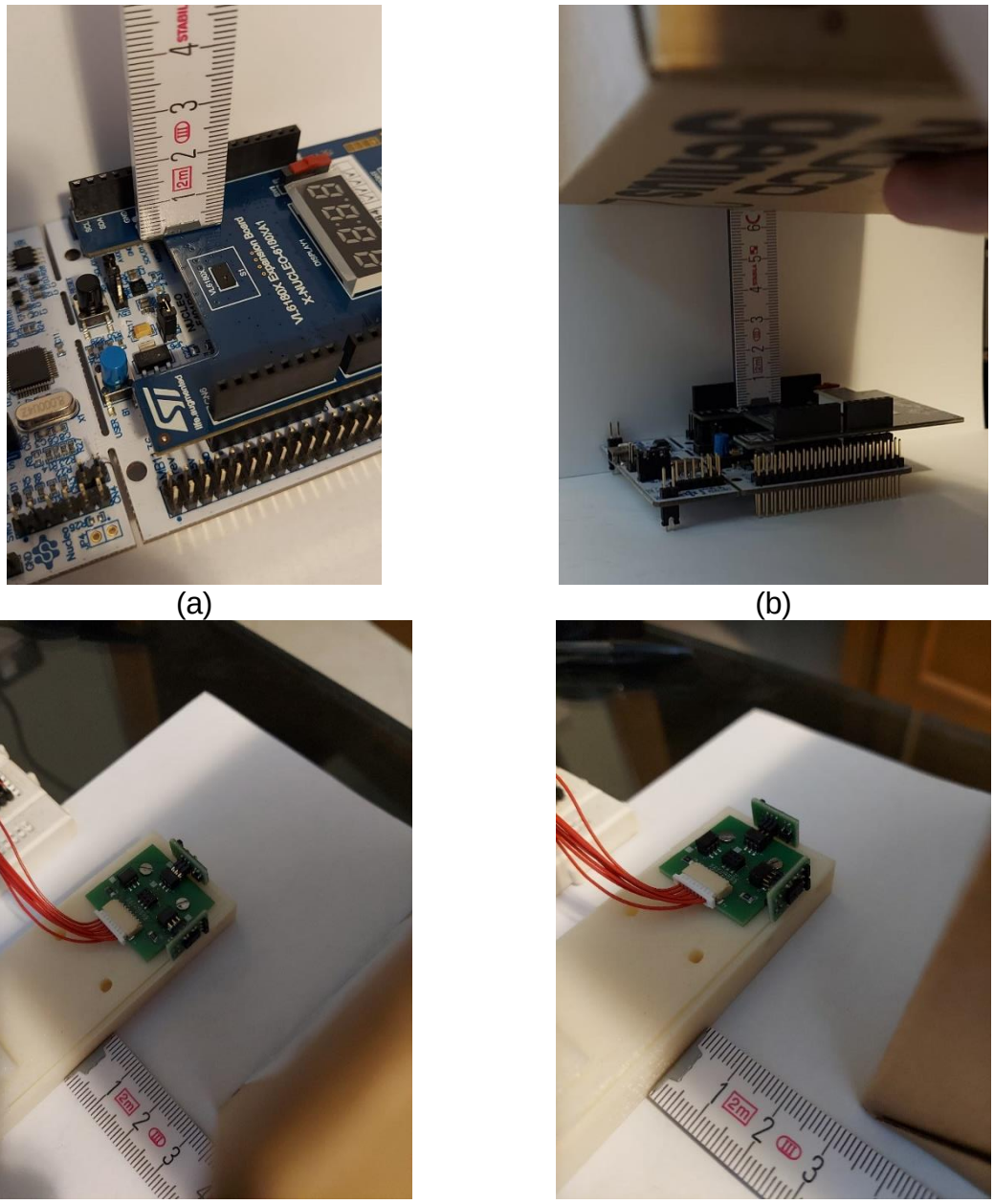

(a) (b)

(c) (d)

Figure 27: Experiment setup for ST Solution (a) and (b) and for custom solution (c) and (d).

6.1 Sampling Frequency

Sampling frequency characterization is of high interest for a Time Of Flight sensor as VL6180X. In such sensors, the sampling frequency highly depends on the convergence time of each measure and, then on the object distance. From datasheet, it can be noticed that the total execution time of a single reading process can be calculated as the sum of:

- Pre-Calibration Time: 3.2 ms,
- Range Convergence Time: variable,
- Readout Averaging Time: 4.3 ms.

The range convergence time depends on the maximum range the sensor is configured for. For example, for a maximum range of 100 mm, the convergence time is 10.73ms with a target reflectance of 3% and 0.73ms with a target reflectance of 88%. In this conditions, typically a reading operation ranges between 8.23ms and 18.23ms that corresponds to a sampling frequency range of [54.8, 121.5]Hz.

Figure 28 reports the sampling frequency for the two systems. In the ST Solution case, the behaviour described at the beginning of this chapter has to take into account. In particular, the sampling frequency reported in Figure 28a refers to the data available before the second filtering stage, so it is not the sampling frequency obtained at the end of the processing channel. In both cases the sampling frequency depends on the obstacle distance: higher the distance lower the sampling frequency. The custom solution shows a more stable behaviour and, in general, a higher sampling frequency when the object distance is around 10cm, e.g., 68Hz.

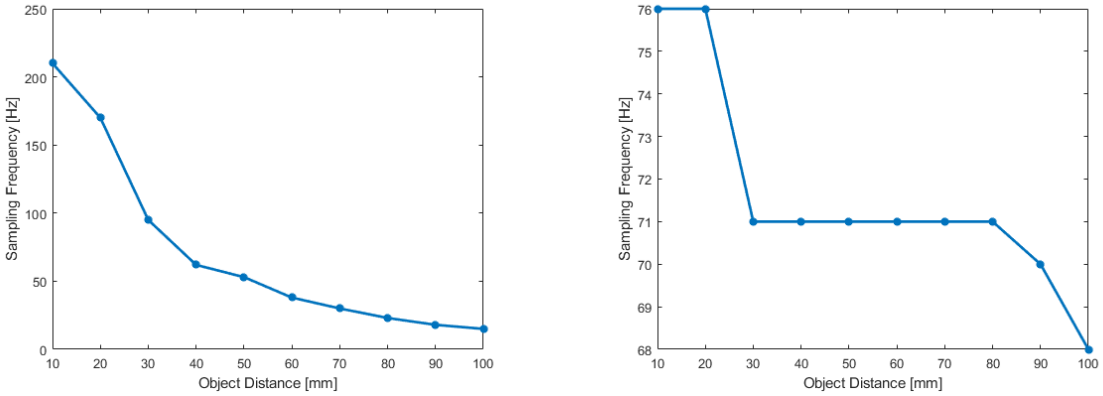

(a) (b)

Figure 28: Sampling frequency for (a) ST solution and (b) sustom solution.

6.2 Repeatability

The repeatability evaluation has been carried out considering a total of 10 measures. During the tests, the object has been moved different times in different positions in order to obtain 10 measures at the following distances: 10 mm, 20 mm, 30 mm, 50 mm, 100 mm. Figure 29 reports the results.The ST solution shows an error that increases when the object is closer to the sensor, e.g., at 10 mm the max error in percentage is 68%. Instead, the repeatability error decreases when the object gets far, e.g., at 100 mm the max error in percentage is 0.72%. For the custom solution, the error is quite constant at the different evaluated object distances. In particular, at 10 mm the max error in percentage is 16% while at 100 mm the max error in percentage is 13%.

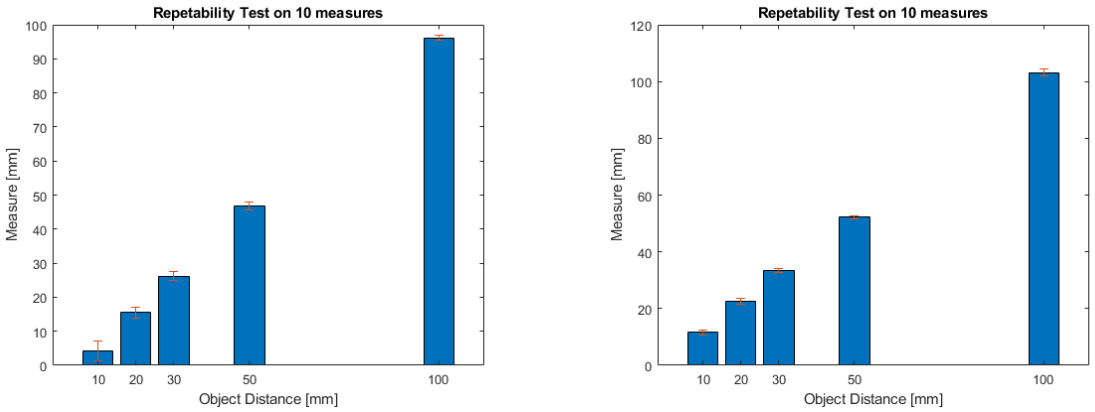

(a) (b)

Figure 29: Repeatability for (a) ST solution and (b) custom solution.

The table below summarizes the repeatability errors in the different working conditions for the two solutions.

Distance [mm]	ST Solution error [%]	Designed Solution error [%]
10 mm	68.59	16.71
20 mm	10.20	15.92
30 mm	4.96	10.52
50 mm	2.36	4.28
100 mm	0.71	3.25

6.3 Hysteresis

Figure 30 reports the hysteresis for the two solutions. The sensor behaviour is quite linear for both solutions and the tests showed the absence of an hysteretical behaviour for VL6180X sensor. The hysteresis error has been computed finding the maximum difference between the distance values on the two "sides" of the hysteresis graph corresponding to the same object distance value and using the following equation:

$$e_{hyst} = \frac{|d_{incr} - d_{decr}|}{d_{max}} \times 100 \quad (4)$$

where d_{incr} and d_{decr} are the distance values on the increasing and decreasing sides respectively and d_{max} is the maximum distance value reached during the experiment. According to the previous equation, the hysteresis errors for the two systems are:

- ST solution hysteresis error: $e_{hyst} = 4.02\%$,
- custom solution hysteresis error: $e_{hyst} = 1.53\%$.

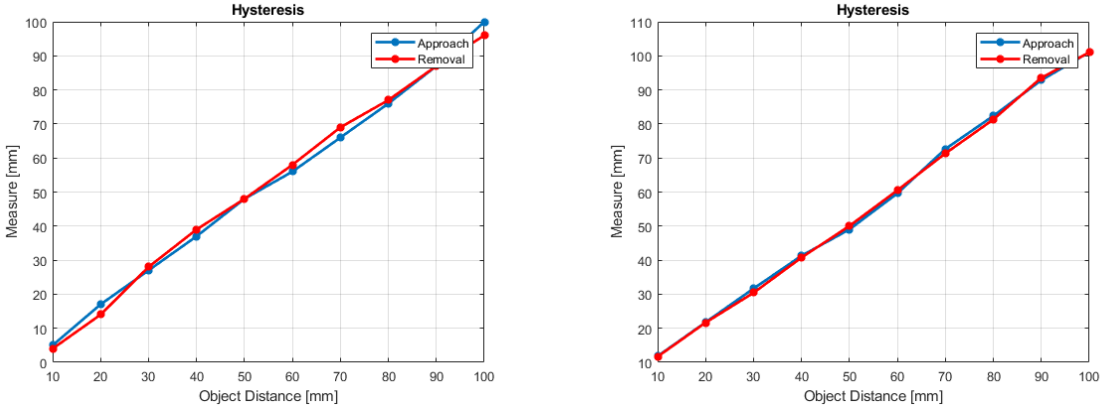

(a) (b)

Figure 30: Hysteresis for (a) ST solution and (b) custom solution.

6.4 Power Spectrum

The power spectrum for two sytems have been computed to evaluate the SNR. The tests have been performed considering the object at different distances in order to evalute if the SNR depends on the object distance. The object has been located at the following distances: 100 mm, 50 mm, 20 mm, 10 mm. The results are reported in Figure 31. It is possible to see how, since the signal bandwidth is limited to few hertz, the noise level is about 4-5 order of magnitude below the signal level in all cases. The noise level for the custom solution is higher than the ST case. It is quite obvious that these results are related to the filtering stages used in the ST processing chain.

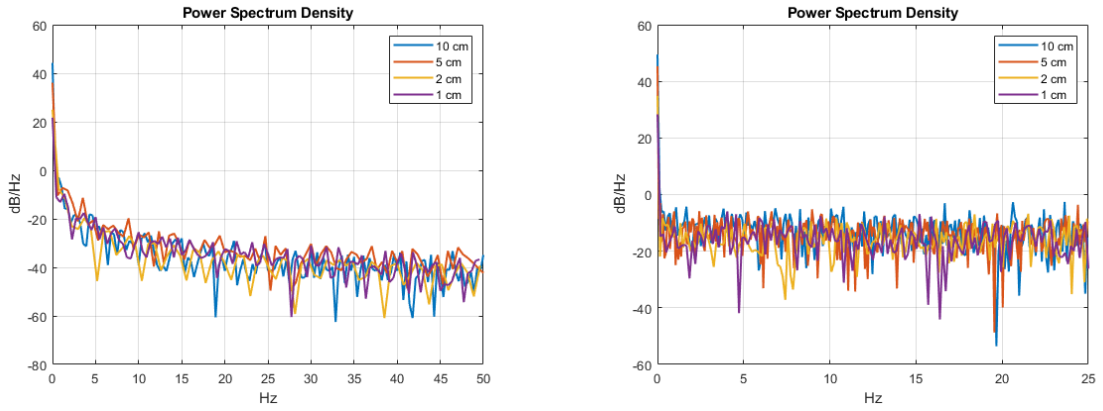

(a) (b)

Figure 31: PSD for (a) ST solution and (b) custom solution.

7 Testing of Sensors in Relation with Use Cases

Regarding the cables manipulation, Figure 32 shows examples of the tactile map obtained when the tactile sensor is in contact with a cable. Exploiting the information given by this map, it is possible to reconstruct, for example, the shape of the cable so to achieve greater dexterity in wire manipulation. Details about the use of tactile data for wire grasping have been already detailed in Deliverable 5.2 – Cable grasping, released in Mo16.

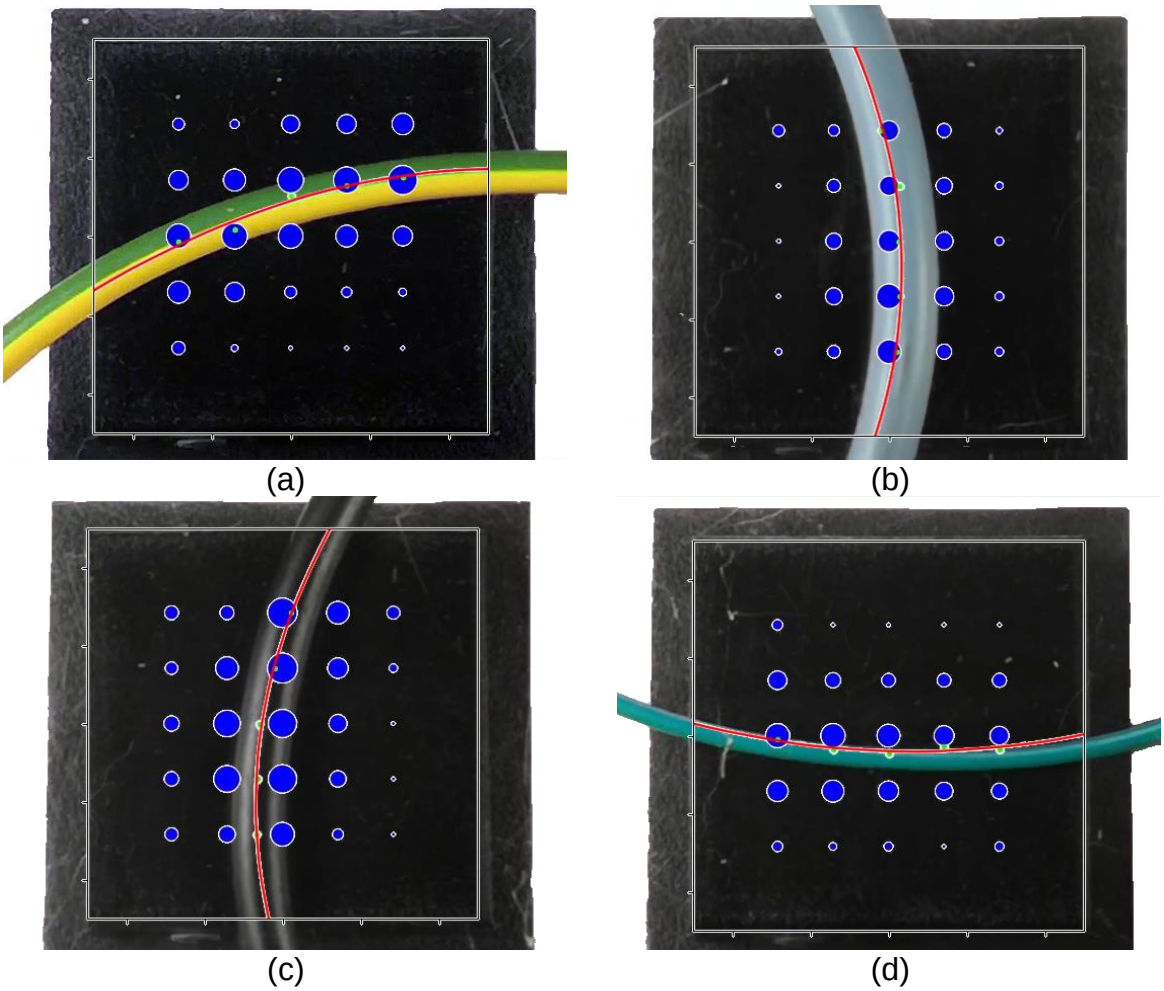

Figure 32: Tactile data used for shape reconstruction of wires with different diameters: (a) wire of 2.5 mm, (b) wire of 4 mm, (c) wire of 3.5 mm and (d) wire of 1 mm.

For the grasping and manipulation tasks on thin and small objects, where the contact area is very small, an accurate knowledge of the object pose is fundamental. As alternative approach to camera, the proximity sensors could be appropriately used, to improve the a priory knowledge of the object pose by re-constructing a proximity-based point cloud. In particular, a specific scanning strategy can be adopted to scan a predetermined area: the measures of the pre-touch sensor, properly processed to be referred w.r.t. to the robot base frame, can be collected in order to obtain the object point cloud. By properly processing the point cloud, the shape of the wire under analysis can be estimated. As showed by the experiments detailed below, the estimated wire shape is very close to the actual wire shape. In particular, the validity of the reconstruction

algorithm has be demonstrated by letting the robot end-effector to automatically follow the wire for all its length through a classical position control. For simplicity, let divide the scanning strategy into two main parts: a) scanning phase and b) shape estimation phase.

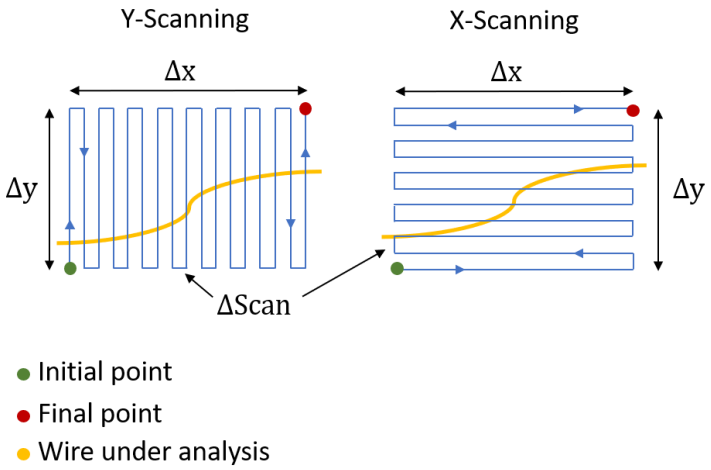

Figure 33: Scanning map generation.

The scanning strategy algorithm has been designed in order to generate a point map by following a trajectory as the ones reported in Figure 33. The shape estimation phase consists in approximating the scanned wire shape by using a third order polynomial. The estimation is realized in three steps: segmentation of the point cloud acquired during the scanning phase in separate rows (or columns); selection of the point with the maximum z-coordinate for each segment; computation of the analytical form of the wire shape estimation by using a third order polynomial interpolation of the points obtained in the previous step. An example of shape estimation is reported in Figure 34, where the red stars are the points with the maximum z-coordinate of the rows in the point cloud and the red line is the third order polynomial approximating the wire shape.

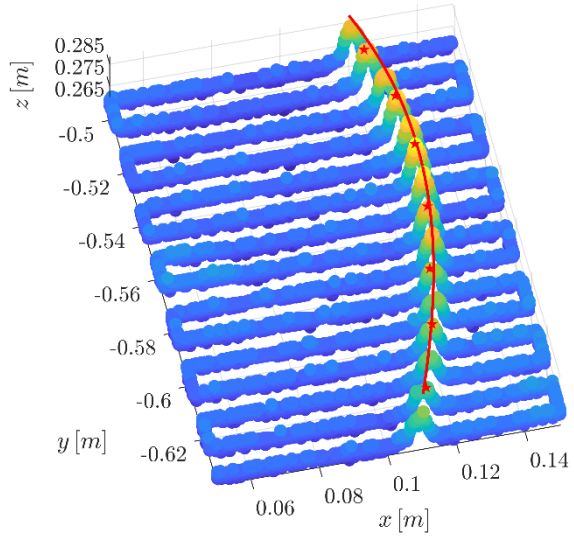

Figure 34: Example of point cloud obtained by using the proximity sensor on a 2.5mm diameter wire.

In order to show how the scanning procedure and the wire shape estimation can be used in a wire manipulation task, a suitable experiment has been carried out. It consists in the robot end effector following the wire for all its length, as shown in the video reported in REMODEL website[1]. To this aim, the trajectory is computed by using the x, y and z coordinates of the estimated wire for the end effector position and the corresponding first derivative for its orientation, so to have the fingers well positioned to grasp the wire. Figure 35 reports some frames from the video showing the robot executing the trajectory explained above. It is important to underline that in a real use case only one grasping point is necessary and it corresponds to one of the points of the trajectory computed for this experiment.

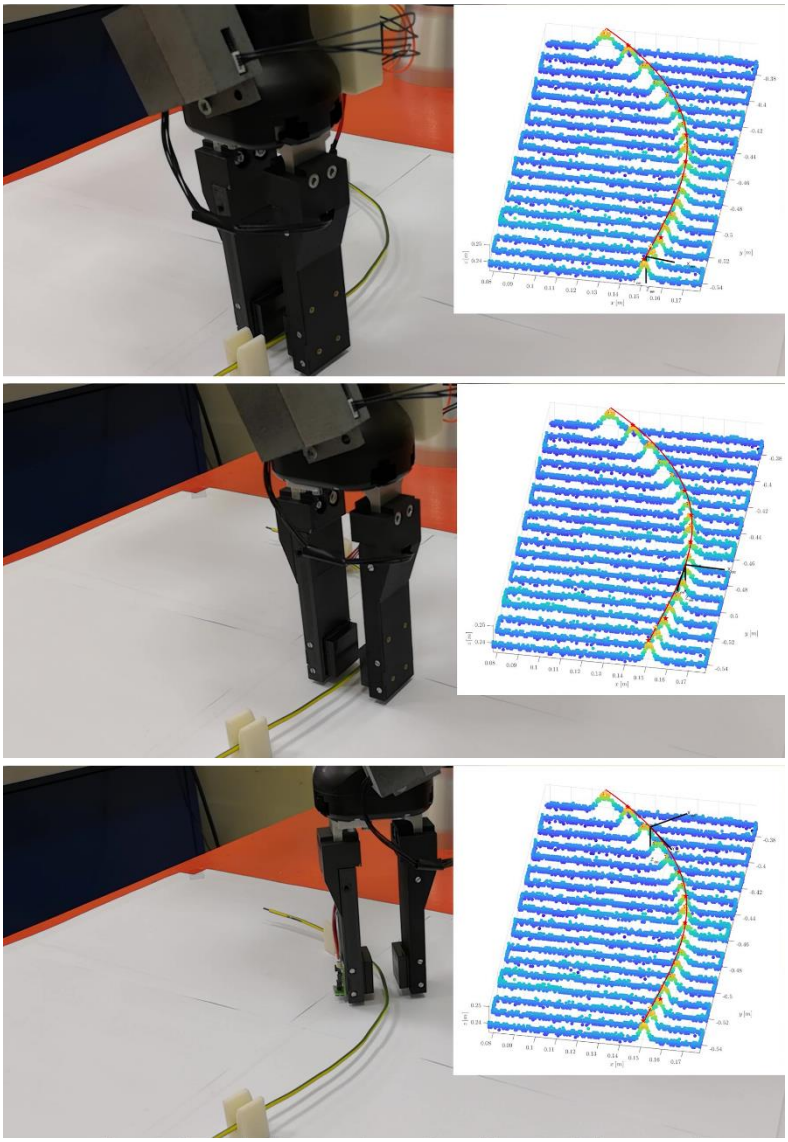

Figure 35: Frames of the video showing the robot end effector following the wire for all its length.

[1] https://remodel-project.eu/sites/remodel.drupal.pulsartecnalia.com/files/Scan%20Wire%20Demo.mp4

8 Conclusions

This document reports all details about the sensor development in REMODEL project. In particular, tactile sensors with 25 taxels, organized as a 5x5 matrix of sensible points, have been developed and integrated into different commercial parallel grippers available in partiners' laboratories. Four couples of sensorized fingers have been delivered to the research partners involved into use cases. The tactile sensors have been deeply characterized in UCLV laboratory, by evaluating their performance in terms of hysteresis, repeatability, response time, signal to noise ratio, sensitivity and sampling frequency. Also the software for the use of sensorized fingers have been developed and released to the other partners, by uploading it into REMODEL GitLab repository. Possible use for the wire grasping is partially reported in this document, while a complete description about their use in wire grasping can be found in the Deliverable 5.2. Additionally to the tactile sensors, proximity sensors based on the use of Time-of-Flight devices have been developed. The sensing system has been designed to be integrated with the tactile sensors previously designed. Each finger can provide up to 4 sensing points. Also in this case both hardware and software heve been developed and released. The sensors have been characterized in terms of hysteresis, sampling frequency, signal-to-noise ratio and repeatability. A possible use to reconstruct the wire shape in the scene by using a suitable scanning strategy is also provided. Several videos about tactile and proximity sensors are available in the corresponding section of REMODEL website.